Journal of Biomechanics 48 (2015) 4221–4228

Contents lists available at ScienceDirect

Journal of Biomechanics

journal homepage: www.elsevier.com/locate/jbiomech
www.JBiomech.com

Mechanical loading up-regulates early remodeling signals from osteocytes subjected to physical damage

Chao Liu [a], Xiaoqing Zhang [b], Michael Wu [c], Lidan You [a,d,*]

[a] Institute of Biomaterials and Biomedical Engineering, University of Toronto, Toronto, ON, Canada
[b] Division of Engineering Science, University of Toronto, Toronto, ON, Canada
[c] Department of Laboratory Medicine and Pathobiology, University of Toronto, Toronto, ON, Canada
[d] Department of Mechanical and Industrial Engineering, University of Toronto, Toronto, ON, Canada

ARTICLE INFO

Article history:
Accepted 18 October 2015

Keywords:
Osteocyte
Physical damage
PGE_2
VEGF
Osteoclastogenesis

ABSTRACT

In the mineralized bone matrix, mechanical loading causes micrometer-sized cracks. These cracks trigger targeted remodeling along the micro-crack. Physical damage to osteocytes was shown to be involved in the initiation of this remodeling process. However, the role of subsequent mechanical loading osteocyte response to physical damage is unclear. In this study, we have designed and developed an *in vitro* cell model to study the impact of mechanical loading on osteocytes with physical damage. Specifically, a system was developed to create sub-cellular physical damage on MLO-Y4 osteocytes *in vitro*. This model re-created the spatial distribution of non-viable cells and VEGF expression around microdamage as reported *in vivo*. Using this system, the short term (24 h) effects of fluid shear stress in regulation of osteocyte response to physical damage were investigated. We have observed that the mechanical stimuli had an additive effect in terms of COX-2, VEGF mRNA expressions, as well as PGE_2, VEGF concentrations in the media. Interestingly, other inflammatory signals such as IL-6 and TNF-α did not change with these stimuli, at this time point. Moreover, fluid shear also had a modulating effect in regulation of osteoclast differentiation by osteocyte with physical damage. These results show that (1) subcellular physical damage upregulates remodeling signals in osteocytes at early time point, (2) mechanical loading substantially upregulates these signals for remodeling in osteocytes with physical damage.

© 2015 Elsevier Ltd. All rights reserved.

1. Introduction

Due to the composite nature of bone, microdamage occurs frequently (Martin, 2003). The microdamage is also repaired readily, which maintains its structural integrity. Recently, it has been shown that remodeling does not occur in microdamaged bone without subsequent mechanical loading (Waldorff et al., 2010). However, the cellular mechanism of how mechanical loading affect bone repair of microdamage is not clear.

Microdamage occurs with diffuse damage proceeding primary micro-cracks (Schaffler et al., 1994; Burr et al., 1997; Frost, 1960). Micro-cracks have more impact on bone quality in terms of fracture toughness (Burr et al., 1997). Also, only micro-cracks trigger targeted remodeling response (Bentolila et al., 1998; Burr et al., 1985; Silva et al., 2006), in contrast to diffuse damages (Herman et al., 2010). In fact, osteonal remodeling preferentially occurs at regions with micro-cracks (Bentolila et al., 1998; Mori and Burr, 1993). Investigation of the cell response to mechanical loading after microdamage would be focused on the effect of micro-cracks.

For micro-cracks, the separation of the bone matrix is in the order of 10 μm (O'Brien et al., 2000; Schaffler et al., 1995; Taylor and Clive Lee, 1998). If such a gap were to occur *in vivo*, it is predicted to cause linear damage across osteocyte process or cell body (Hazenberg et al., 2006).

Osteocytes are suggested to be responsible in sensing and controlling microdamage-induced remodeling (Noble et al., 2003a; Parfitt, 1994; Herman et al., 2010). Decline in osteocyte density have shown to result in accumulation of microdamage (Vashishth et al., 2000b). Osteocyte malfunction (Phillips et al., 2008) or absence (Tatsumi et al., 2007) in mouse models leads to bone fragility consistent with that observed in aging and osteoporosis. Specifically, while osteocyte ablation increased bone resorption in mice under physiological loading, the same mice were resistant to the disuse-induced bone loss when their hind

* Correspondence to: 164 College Street, Room 407, Toronto, ON, Canada M5S 3G9.
E-mail addresses: ccc.liu@mail.utoronto.ca (C. Liu), xiaoqing.zhang@mail.utoronto.ca (X. Zhang), jvlichael.wu@mail.utoronto.ca (M. Wu), youlidan@mie.utoronto.ca (L. You).

http://dx.doi.org/10.1016/j.jbiomech.2015.10.018
0021-9290/© 2015 Elsevier Ltd. All rights reserved.

limbs were subjected to unloading (Tatsumi et al., 2007). *In vivo*, apoptotic osteocytes were observed near the microdamage sites (Cardoso et al., 2009). In fact, microdamage have been observed to be initiated from lacunae, which house osteocytes (Reilly, 2000).

Under mechanical loading, osteocytes alter their expression of soluble factors that control bone remodeling (Henriksen et al., 2009; Noble et al., 2003b; Robling et al., 2006). Mechanical loading decreases osteocyte apoptosis induced by TNF-α treatment (Cheung et al., 2012). Furthermore, osteocyte apoptosis could induce osteoclast recruitment (Aguirre et al., 2006; Burger et al., 2003) and differentiation (Al-Dujaili et al., 2011). Conversely, osteocytes that have been subjected to fluid flow shear stress (FFSS) inhibit osteoclast formation and bone resorption (Tan et al., 2007; You et al., 2008). In osteocytes, prostaglandin E2 (PGE_2) could be mechanically induced (Ajubi et al., 1996). PGE_2 stimulates both resorption and formation (Bergmann and Schoutens, 1995; Raisz et al., 1993). Cyclooxygenase-2 (COX-2) is involved in the production of PGE_2 (Ponik et al., 2007). COX-2 was up-regulated after fluid flow (Ponik et al., 2007) and fluid pressure (Liu et al., 2010) in MLO-Y4 osteocytes. Vascular endothelial growth factor (VEGF), is expressed in osteocytes. It is upregulated in regions of bone with micro-cracks and correlates with apoptotic osteocytes (Kennedy et al., 2012). VEGF could be regulated by mechanical loading indirectly (Cheung et al., 2011). Interestingly, *in vivo* studies showed that bone with fatigue-induced micro-cracks has increased levels of bone remodeling-related genes COX-2, and VEGF (Kidd et al., 2010).

Since osteocytes are the major mechanosensor cells in bone (Bonewald and Johnson, 2008; Riddle and Donahue, 2009), their response to micro-cracks could also be mechanically regulated. We hypothesize that after physical trauma as in the case of micro-cracks in bone, mechanical loading regulates osteocyte production of early remodeling related molecules: PGE_2 and VEGF. A system was created to achieve sub-cellular physical damage (PD) to cells similar to the effect of micro-cracks. Osteocyte expression of signaling molecules involved in the initiation of bone remodeling were quantified. The capacity of damaged and mechanically stimulated osteocytes to induced osteoclast differentiation was investigated.

2. Methods

2.1. Osteocyte cell model

MLO-Y4 osteocyte-like cells (gift from Dr. Lynda Bonewald, University of Missouri) were cultured in α-MEM supplemented with 2.5% fetal bovine serum, 2.5% calf serum, and 1% penicillin–streptomycin (Invitrogen) on type I rat tail collagen-coated plates at 37 °C and 5% CO_2. The cells were seeded onto collagen-coated glass slides and grown to 80% confluence.

2.2. Osteocyte physical damage model

A system was developed to apply consistent level of PD to cells cultured on a 2D substrate (Fig. 1). This system consists of a horizontal aluminum bar suspended on top of two T-sections. A carriage on the horizontal bar was free to move in one direction horizontally. The carriage has a clamp, which holds 4 tungsten needles with 1 μm tip size (Roboz Inc). The vertical position of the clamp is adjustable *via* an M4 screw. One rotation corresponds to 0.4 mm vertically. The tungsten needles were used to introduce PD to MLO-Y4 cells. The contact of the needle to the glass slide was confirmed visually. The path of the damage is typically 1–10 μm in width, and either 38 or 75 mm in length (dimensions of a glass slide). The cell culture was damaged to have ~15% dead cells.

2.3. Cell viability staining and quantification

Cell damage was assessed with Trypan Blue dye (Sigma) method from previous study on MLO-Y4 cell viability (Plotkin et al., 1999). Trypan Blue would penetrate apoptotic and necrotic cells, while excluded by cells with intact membrane. After cellular damage, the samples were washed once with PBS (Gibco). Then, 0.04% Trypan Blue dye in PBS was applied to the cells on glass slides. The x, y coordinates of positively stained cells were recorded in each field of view. The damage sites were represented by a linear function, $y=mx+b$, where m is slope and b is y intercept. The distance of each positively stained cell to the closest damage site was calculated. Each field of view had at least 3 damage sites and 1000 cells. The experiment was repeated four times, with at least 5 samples per experiment.

Live/Dead assay (Invitrogen) was performed on damaged MLO-Y4 cells according to manufacture instructions. Fluorescent microscope (Nikon) was used to image the slides for calcein AM, and Ethidium homodimer-1, for live and dead cells, respectively. The number of live and dead cells was counted in each field of view. Each field of view had at least 3 damage sites and 1000 cells. The experiment was repeated four times, with at least 5 samples per experiment.

2.4. Fluid shear stress treatment

Parallel flow chambers were used to apply oscillatory FFSS as previously described (Jacobs et al., 1998; You et al., 2008) to the physically damaged cells. Assuming viscous flow in parallel plate chamber, the FFSS on the cells is expressed as $\tau=6\mu Q/(bh^2)$ where τ is the shear stress; μ is the viscosity of the medium, which is approximated to be that of the water at room temperature (1×10^{-3} Pa s); Q is the maximum flow rate during oscillatory flow (0.5 ml/s); b is the channel width (35 mm); h is the channel height (0.4 mm).

Cells in all conditions were placed into flow chamber for the duration of the experiment. Fluid flow was applied by a 3 ml plastic syringe (BD), which is driven by a linear actuator. The flow was oscillatory with sinusoidal profile at frequency of 1 Hz, and applied peak FFSS of 2 Pa to the cells. After physical damage, FFSS was applied for 1 h. Then the slides were incubated with fresh media for 23 h. This experiment was repeated for at least three times for each assay.

2.5. mRNA expression quantification

Total RNA was isolated from MLO-Y4 cells at 6, 8 and 24 h after flow treatment. Reverse transcription was performed with Superscript III (Invitrogen). The resulting cDNA samples were subjected to quantitative PCR with SYBR Green I (Roche) for genes IL-6, TNFα, COX-2, VEGF, RANKL, and OPG. Mastercycler ep realplex2 (Eppendorf AG) was used to run the Real-time PCR machine. Expression levels of each gene were normalized to the housekeeping gene 18 s.

2.6. Protein expression quantification

Levels of VEGF and PGE_2 were measured in the media from the post-flow incubation (24 h). VEGF was measured with ELISA kits (Mouse VEGF ELISA Duo Set, R&D Systems). PGE_2 levels were measured with EIA kits (Cayman Chemical).

2.7. VEGF immunostaining

After PD, MLO-Y4 cells were incubated for 30 min. Then the cells were fixed with 3% paraformaldehyde (Sigma) for 15 min. PBS was used as wash buffer for three times at 5 min each for each wash. The cells were blocked and permeabilized with 1% BSA in 0.1% PBS-Tween 20 (Sigma) for 1 h. Rabbit anti-mouse VEGF antibody was diluted in the blocking/permeabilization buffer to 5 μg/ml, and applied to the cells for 16 h at 4 °C. Goat Anti-Rabbit fluorescently labeled antibody was diluted in the blocking/permeabilization buffer to 10 μg/ml, and applied to the cells for 1 h at room temperature. The nuclei were labeled with DAPI.

The intensity of VEGF staining in each cell was quantified by measuring the integrated density of the cell in ImageJ. The background intensity was calculated by multiplying the mean density of three adjacent empty regions by the cell area. This background intensity was subtracted from the integrated intensity of each cell to correct for background.

2.8. Osteoclast differentiation of RAW 264.7 in conditioned media and TRAP staining

RAW264.7 cells were cultured in growth media until 70% confluence. The growth media consists of DMEM (Sigma) with 10% FBS (Gibco), 1% P/S (Gibco), 4 mM L-glutamine (Sigma). Then the cells were cultured in differentiation media for 7 days. The differentiation media was growth media with 25 ng/ml RANKL (R&D Systems), which was mixed 1:1 with conditioned media from MLO-Y4 cells that had been subjected to combinations of PD and fluid shear. Media was changed daily. After 7 days of differentiation, the cells were fixed and stained for tartrate-resistant acid phosphatase (TRAP), which is only expressed in osteoclasts. TRAP positive cells with three or more nuclei were quantified under bright field microscope (Zeiss).

2.9. Statistical analysis

Factorial ANOVA is used to investigate the interaction effect of fluid flow and PD. In experiments with two stimuli: fluid flow shear and PD, a 2^2 factorial design was used to investigate the effect of individual stimulus as well as their interactive effects. The statistical software JMP was used for this analysis.

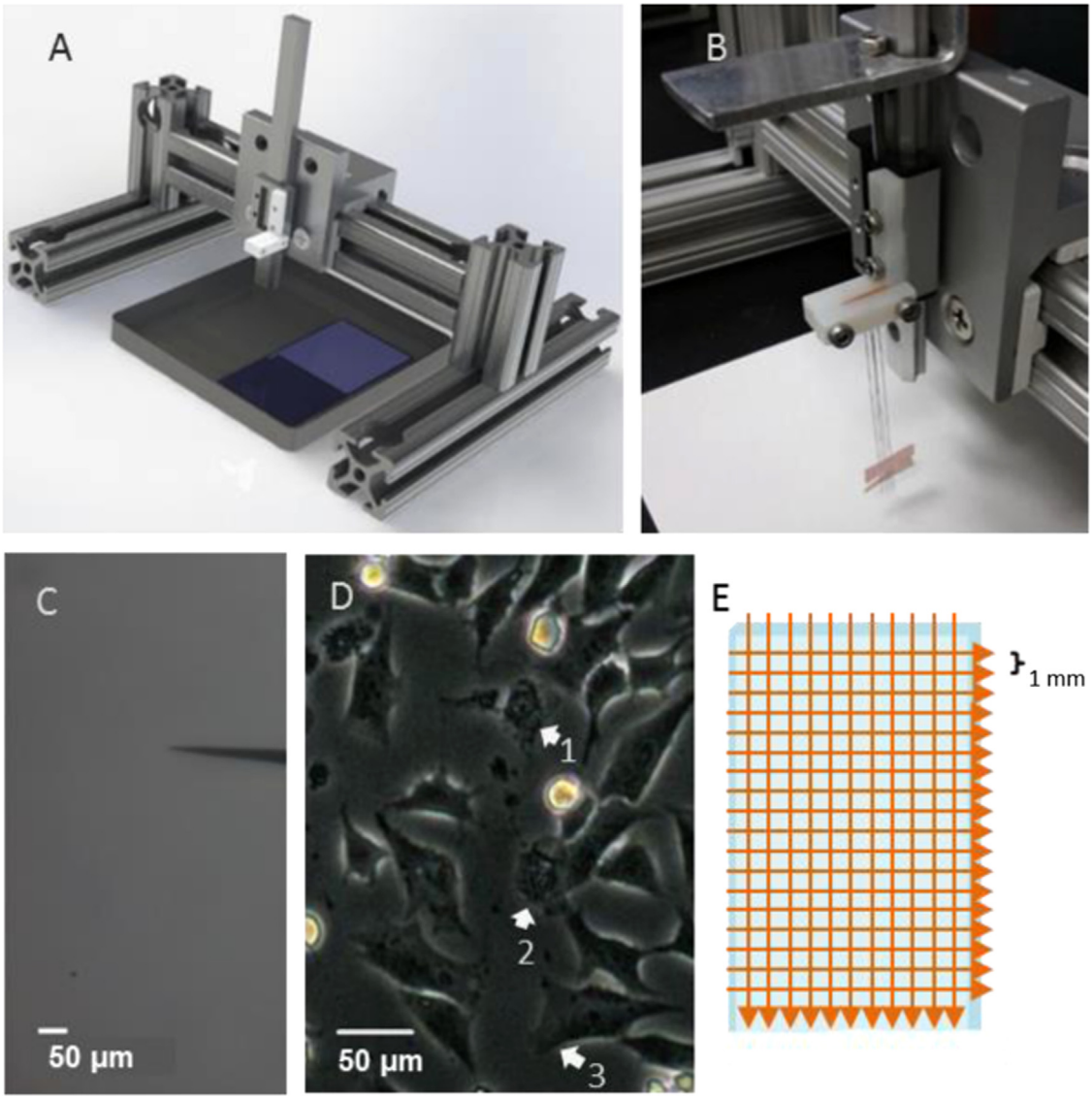

Fig. 1. A rail and carriage system to attach 1 μm tipped needles. It allows for smooth horizontal movement and fine vertical position control. Passage of the needles caused rupture of cell membrane. (A) System render in CAD software. (B) Screw controls vertical position: 1 turn = 0.4 mm. The array of 4 needles is 4 mm across. (C) Microscope photo showing tip dimension of micro-needle. (D) Typical damage caused by the system. Arrow 1 indicates a cell that was damaged through the cytoplasm. Arrow 2 indicates a cell that was damaged through the nucleus. Arrow 3 indicates a cell with damaged process. (E) Paths of damage on glass slide consist of length-wise and width-wise cuts across the slide. There are 74 damage sites across the length of the slide, and 37 across the width.

3. Results

3.1. Osteocyte physical damage model validation

The capability of the cell damage system was assessed through observation of damaged cells, and viability staining. The cell damage system was able to damage MLO-Y4 cells cultured on glass slides. The linear damage was induced across the glass slides (75 mm × 38 mm) as shown in Fig. 1E.

The tungsten needles were pliable enough to be bent, which created damage larger than 1 μm. The unevenness of the glass slide, at the micron scale, contributed to this variation. With this system, damage site width was controlled to be within the range of 1–10 μm.

Since the *in vivo* cultured cells are randomly distributed over the slides, different parts of the cells were damaged depending on their relative position to the damage site. Various parts of the cell were cut through during the damage process, including nucleus, part of the cell body, and the processes (Fig. 1D). A significant number of dead cells was observed near the damage sites using Trypan Blue and Live/Dead assay (Fig. 2A and B). Most Trypan blue stained cells were within 150 μm of the nearest damage site (Fig. 2C). The density of Trypan blue stained cells was significantly higher within 150 μm of the damage site compared to area that is further away (Fig. 2D).

3.2. mRNA expression 24 h after cell damage

Changes in transcription of remodeling-related genes: IL-6, TNFα, COX-2, RANKL, and OPG were measured by quantifying their mRNA levels. From all cells in each sample, COX-2 and VEGF mRNA levels significantly increased only at 24 h after cell damage (Fig. 3). RANKL, OPG, IL-6, and TNF-α mRNA levels were not changed at the time points tested (data not shown). From each individual stimulus, the increase in COX-2 and VEGF was over 1.5 fold over control. FFSS after PD induced greater than 3 fold increase in COX-2 and VEGF mRNA over control (Fig. 4) 24 h after PD to the cells.

3.3. Concentration of PGE_2 and VEGF in media 24 h after cell damage

The concentration of PGE_2 and VEGF in media showed similar level of increase to the corresponding gene expressions for COX-2 and VEGF at 24 h after cell damage. With only PD, the increases in PGE_2 and VEGF were not significantly different from control. With only FFSS, PGE_2 was not significantly different from control; VEGF showed a 2 fold increase. FFSS after PD induced 5 fold increase in PGE_2, and 3 fold increase in VEGF over control (Fig. 5).

3.4. VEGF immunostaining of damaged MLO-Y4 cells

The location and change of VEGF production in osteocytes are indicative of angiogenesis. While VEGF is ubiquitously expressed in MLO-Y4 cells, its expression was locally elevated near the damage sites (Fig. 6A). The intensity of VEGF staining could be as high as 2.6 times higher compared with the baseline expression. The elevated VEGF expression drops as a function of the distance to the damage sites. For cells more than 150 μm from a damage site, the VEGF expression had dropped to baseline level. Cells that were within 150 μm from a damage site had over two fold increase in intensity of VEGF (Fig. 6B).

3.5. Effect of osteocyte conditioned media on osteoclasts differentiation

RAW264.7 cells were cultured with conditioned media from MLO-Y4 cells that were subjected to either FFSS and/or PD. TRAP positive cells are most numerous in the control group, lower in the physically damaged group, and very low in the flow only and flow+damage groups (Fig. 7). Media from damaged MLO-Y4 cells produced a threefold reduction in osteoclast number. FFSS conditioned media abolished the formation of osteoclasts. The combination of PD and FFSS induced increased number of osteoclast comparable to FFSS only, but the difference in means was not statistically significant.

4. Discussions

In this study, we have developed an *in vitro* osteocyte physical damage model that allows the application of controlled fluid shear mechanical loading to physically damaged osteocytes for measurement of short term (24 h) response. Specifically, to simulate the PD of microcracks on osteocytes comparable to what occurs *in vivo* (Hazenberg et al., 2006), our system was able to induce arrays of linear damage to the cells. The damage induced by our device was able to cause sub-cellular damage to the MLO-Y4 osteocytes cultured on glass slides. The damage profile with respect to the cell components is indiscriminate. The effectiveness and validity of our *in vitro* osteocyte PD model were measured by the spatial distribution of non-viable osteocytes and expression of VEGF. This model reproduced the loss in cell viability as seen from *in vivo* observations (Cardoso et al., 2009; Kennedy et al., 2012). We have observed that mechanical loading in the form of FFSS dramatically increased the level of remodeling initiation signals produced by osteocytes.

Previous study had shown an *in vitro* physical damage model for MLO-Y4 osteocyte-like cell line (Kurata et al., 2006). The cells were embedded in collagen–Matrigel mixture. A 21-gauge needle was then used to cause damage to the gel and the embedded cells. However with the cells embedded in gel, controlled fluid flow shear loading could not be applied to the cells. The system

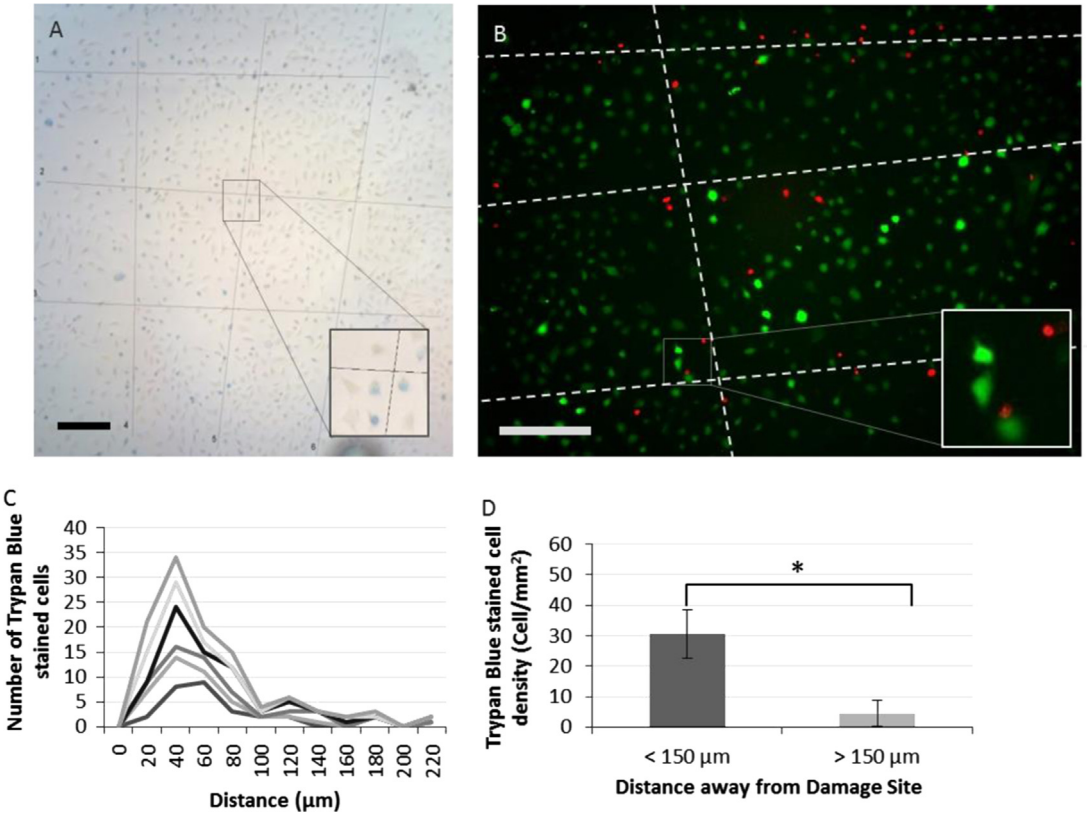

Fig. 2. (A) Trypan Blue staining showed uptake of the dye near the damage sites (labeled with lines). The inset shows a magnified area with stained (blue) and non-stained cells (B) LIVE/DEAD staining of damaged MLO-Y4 cells was used to quantify the percentage of cells that have sustained damage. Live and dead cells are labeled green and red respectively. The inset shows a magnified area with live and dead cells. (C) A representative plot of six samples for the number of cells (stacked) as a function of distance to the damage site. (D) Trypan Blue-positive cell density was quantified vs. distance to closest damage sites. Data shown are mean ± standard deviation. (*$p < 0.05$, A scale bar=50 μm, B scale bar=250 μm). (For interpretation of the references to color in this figure legend, the reader is referred to the web version of this article.)

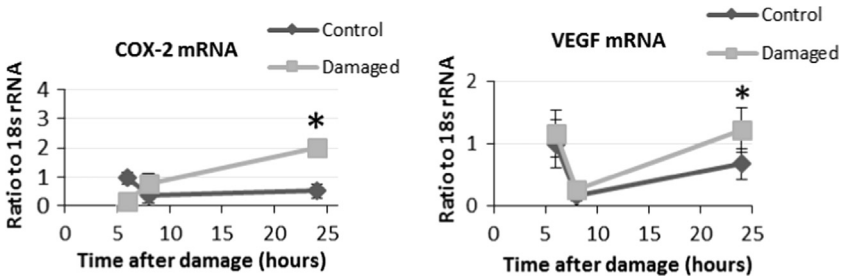

Fig. 3. Time-point response of MLO-Y4 cells to physical damage without fluid shear stress ($n=6$). mRNA levels of VEGF and COX-2 are elevated 24 h after damage in MLO-Y4 cells. Data shown are mean ± standard deviation.

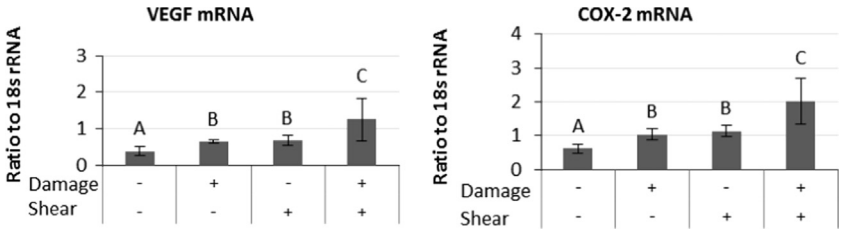

Fig. 4. MLO-Y4 cell response to the combinations of physical damage and fluid shear stress in terms of mRNA expression of VEGF and COX-2 ($n=3$). Means that do not share a letter are significantly different. Data shown are mean ± standard deviation.

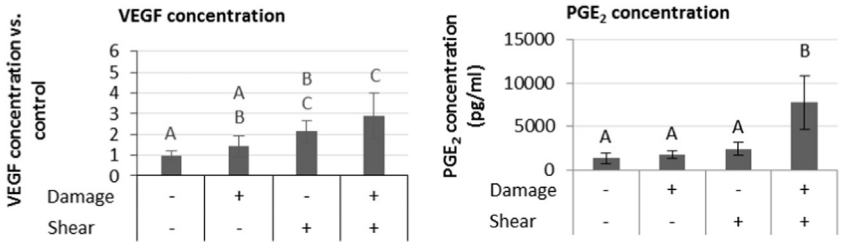

Fig. 5. MLO-Y4 cell response to the combinations of physical damage and fluid shear stress in terms secreted VEGF and PGE_2 24 h after damage ($n=3$). Means that do not share a letter are significantly different. Data shown are mean ± standard deviation.

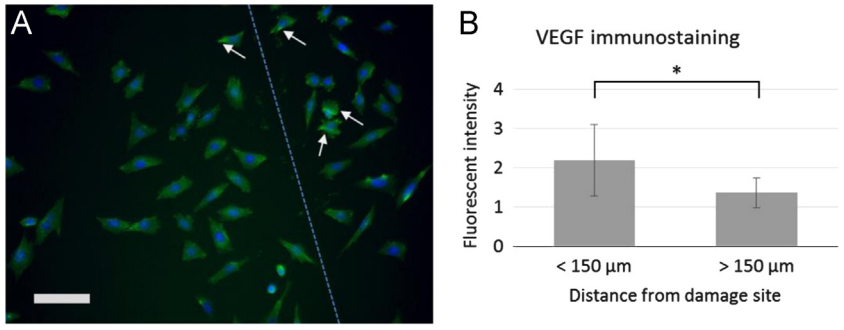

Fig. 6. (A) VEGF immunostaining of MLO-Y4 cells 30 min after physical damage, colored green. Nuclei were stained with DAPI, shown as blue. White arrows indicate locally increased VEGF expressions near damage sites, shown by dotted lines. Scale bar=50 μm. (B) The average VEGF intensity of cells that are within 150 μm of damage sites or outside of this range. Data shown are mean ± standard deviation (For interpretation of the references to color in this figure legend, the reader is referred to the web version of this article.)

developed in our study allows application of FFSS to the cells with PD. One caveat of this system is that the three dimensional morphology of the osteocyte and the dimension order of its surrounding matrix could not be captured. Another caveat is the matrix bound signaling molecules that would have been released in micro-crack are not included. Nonetheless, this model provides a first step in studying the effect of mechanical loading on osteocyte with physical damage. In future studies, it could be adapted to distinguish various additional stimuli such as substrate dimension and matrix bound signals.

Kurata et al. have reported that the damaged MLO-Y4 cells secreted increased levels of macrophage-colony stimulating factor (M-CSF) and RANK; and induced TRACP expression in co-cultured bone marrow cells after 7 days of culture (Kurata et al., 2006). A latter study, using the same model, has shown increased RANKL and decreased OPG secretion (Mulcahy et al., 2011). We have not seen similar increase in RANKL. This is likely due to time point of the observation. We have shown a model for short term (24 h) response by osteocyte here. Whereas with the previous model, the time point was 7 days.

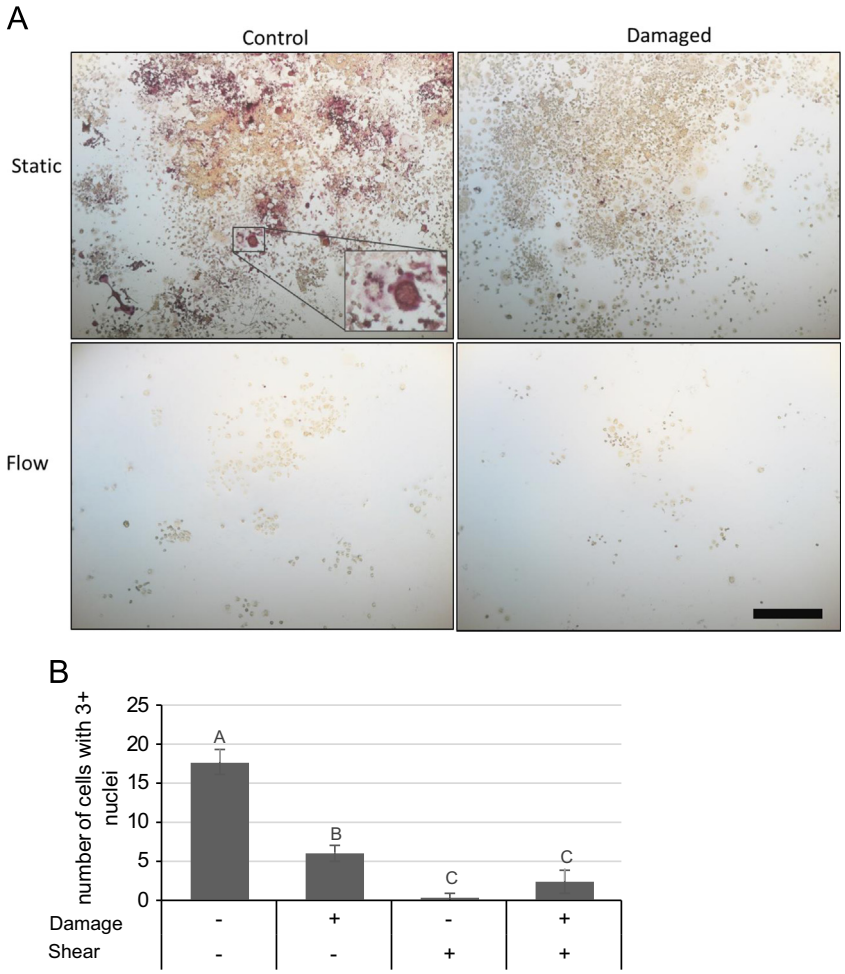

Fig. 7. (A) TRAP staining of differentiated RAW 264.7 cells cultured in conditioned media from MLO-Y4 cells with combination of physical damage and fluid flow shear stress. Horizontal and vertical labels indicate the stimuli applied to MLO-Y4 cells, from which the conditioned media was used to culture RAW 264.7 cells. Scale bar = 100 μm. Inset showing multinucleated TRAP+ cells. (B) Quantification of TRAP staining of RAW 264.7 cells differentiated with MLO-Y4 conditioned media. The number of cells that are TRAP+ and has 3+ nuclei was counted. Means that do not share a letter are significantly different. Data shown are mean ± standard deviation.

It could be argued that the damaged osteocyte population produced by our system could be a model for osteocytes in bone fracture. However we have controlled the viable osteocyte population to be 86–84%, while osteocyte viability in long bone fracture is from 25% to 58% (Dunstan et al., 1993). In fatigue loaded rat long bone, osteocyte viability is around 80% (Verborgt et al., 2000), which was very close to our condition. This is in contrast to healthy bone tissue, which has more than 95% viable osteocytes (Dunstan et al., 1993). Though direct evidence of osteocyte being physically damaged by micro-crack is few (Hazenberg et al., 2006), our model was able to simulate the loss of viability similar to osteocytes near micro-cracks *in vivo*.

Fatigue loading *in vivo* could induce loss of osteocyte integrity localized (within 150 μm) to the region of bone containing micro-cracks (Kennedy et al., 2012). The spatial distribution of dead cells in our system (Fig. 2C and D) approximates that of the *in vivo* fatigue loading study. Osteocyte apoptosis is well known to be critical in the initiation of bone remodeling (Aguirre et al., 2006; Cheung et al., 2011).

The importance of VEGF to bone remodeling had been highlighted in the case of fracture repair (Ito et al., 2005). VEGF increases vascular permeability, allowing progenitors to enter into the remodeling site (Ferrara et al., 2003). In these ways, VEGF is required in the initiation of the BMU (Smith and Calvi, 2013). Also VEGF has been shown to regulate osteoblast survival (Street and Lenehan, 2009). Therefore, the spatial distribution of VEGF expression level is critical to the directionality of bone remodeling. We have found that the VEGF expression in cells around the damage sites approximate that produced *in vivo* (Kennedy et al., 2012) in terms of the distance of cells with higher expression level relative to the damage site. Up-regulation of VEGF mRNA and consequently, medium concentration levels would have been significant in creating a gradient to direct angiogenic sprouting (Shin et al., 2011).

In fracture repair, COX-2 and consequently PGE_2 have been shown to be vital for remodeling (Xie et al., 2008). The PGE_2 level (~8000 pg/ml) from the combination of FFSS and PD was in the range (> 3520 pg/ml) to cause osteogenic effect in bone marrow stromal cells, whereas the PGE_2 levels in other groups were not (Keila et al., 2001). The PGE_2 concentration has increased nearly 2 fold under FFSS *vs.* control. PGE_2 concentration is sensitive to duration as well as magnitude of loading, and the relationship has shown to be non-linear (Kamel et al., 2010). For FFSS treated cells, the discrepancy between our PGE_2 observation and other studies was likely caused by the time point at which the media PGE_2 level was measured.

PGE_2 up-regulates VEGF in osteoblasts (Harada et al., 1994). Also, PGE_2 has been shown to be upstream of the β-catenin pathway, which controls VEGF expression in osteocytes (Kitase et al., 2007). Conversely VEGF promotes late COX-2 protein induction (Clarkin et al., 2008), which may explain the result of increased COX-2 mRNA and PGE_2 concentration 24 h after treatment observed in this study. The coincidental increase in both PGE_2 and VEGF at the 24 h point hints at a

positive feedback loop that increases the concentration of both signals in preparation for establishing the BMU.

IL-6, TNF-α mRNA levels did not change in response to PD, suggesting that osteocytes may not be responsible for the changes in these genes that were observed within 24 h of bone fatigue damage *in vivo* (Kidd et al., 2010). A limitation in our study is the *in vitro* nature of the experiments. MLO-Y4 cells express many markers of osteocytes (Bonewald, 1999). But MLO-Y4 cells express many proteins at different levels *vs.* primary cells (Yang et al., 2009). This 2D culturing substrate could affect cell attachment, which affects cell strain under FFSS (You et al., 2001). With *in vitro* system, dissolved signaling molecules could readily diffuse over the culture. This process would have been much slower *in vivo* due to the lower permeability of the lacuna–canalicular space (Goulet et al., 2009). Osteocytes also produce other factor at different stages of bone remodeling, including RANKL, OPG, sclerostin, and osteocalcin. Mechanosensitivity of these factors in damage osteocytes should be investigated in the future.

Cracks in bone tend to propagate from existing cracks (Bonfield et al., 1978), where remodeling may be already taking place (Waldorff et al., 2010). Also, micro-cracks tends to form ahead of propagating macro-cracks (Vashishth et al., 2000a). Osteocytes signaling in response to micro-cracks may have an effect on existing remodeling processes, specifically, osteoclast differentiation. In this study, signals from osteocytes subjected to FFSS reduced the number of osteoclasts, as has been well established in the literature (Tan et al., 2007; You et al., 2008). Osteocyte response to mechanical loading seems to have a dominant effect on osteoclast differentiation, since media from osteocytes subjected to combinations of PD and FFSS reduced the number of osteoclast to the same level of FFSS alone (Fig. 7B). Our results point to an inhibitory effect of osteocytes with PD on osteoclast differentiation shortly (24 h) after the onset of osteocyte PD. In contrast, the evidence of RANKL production by osteocyte near microdamage is obtained for 3-day (Kennedy et al., 2012) and 7-day (Kurata et al., 2006) time points. The inhibitory effect of microdamage on osteoclastogenesis may be transient, and only occurs shortly after microdamage.

An *in vitro* osteocyte physical damage model was developed that enables investigation of mechanical regulation of osteocyte response to micro-crack induced cellular damage. FFSS loading after PD increased osteocyte expression of inflammatory (COX-2) and angiogenic (VEGF) genes, as well as the corresponding released molecules (PGE_2, VEGF) after 24 h, which are higher than that from each stimulus alone.

Conflict of interest statement

The authors have no conflict of interest.

Acknowledgment

This work was funded by Natural Sciences and Engineering Research Council of Canada (NSERC) Discovery Grant (315868), and Canadian Institutes of Health Research (CIHR) (173865). The funding agencies had no involvement in the study design, in the collection, analysis and interpretation of data; in the writing of the manuscript; and in the decision to submit the manuscript for publication.

References

Aguirre, J.I., Plotkin, L.I., Stewart, S.A., Weinstein, R.S., Parfitt, A.M., Manolagas, S.C., Bellido, T., 2006. Osteocyte apoptosis is induced by weightlessness in mice and precedes osteoclast recruitment and bone loss. J. Bone Miner. Res. 21, 605–615.
Ajubi, N.E., Klein-Nulend, J., Nijweide, P.J., Vrijheid-Lammers, T., Alblas, M.J., Burger, E.H., 1996. Pulsating fluid flow increases prostaglandin production by cultured chicken osteocytes – a cytoskeleton-dependent process. Biochem. Biophys. Res. Commun. 225, 62–68.
Al-Dujaili, S.A., Lau, E., Al-Dujaili, H., Tsang, K., Guenther, A., You, L., 2011. Apoptotic osteocytes regulate osteoclast precursor recruitment and differentiation in vitro. J. Cell. Biochem. 112, 2412–2423.
Bentolila, V., Boyce, T., Fyhrie, D., Drumb, R., Skerry, T., Schaffler, M., 1998. Intracortical remodeling in adult rat long bones after fatigue loading. Bone 23, 275–281.
Bergmann, P., Schoutens, A., 1995. Prostaglandins and bone. Bone 16, 485–488.
Bonewald, L.F., 1999. Establishment and characterization of an osteocyte-like cell line, MLO-Y4. J. Bone Miner. Metab. 17, 61–65.
Bonewald, L.F., Johnson, M.L., 2008. Osteocytes, mechanosensing and Wnt signaling. Bone 42, 606–615.
Bonfield, W., Grynpas, M.D., Young, R.J., 1978. Crack velocity and the fracture of bone. J. Biomech. 11, 473–479.
Burger, E.H., Klein-Nulend, J., Smit, T.H., 2003. Strain-derived canalicular fluid flow regulates osteoclast activity in a remodelling osteon – a proposal. J. Biomech. 36, 1453–1459.
Burr, D.B., Martin, R.B., Schaffler, M.B., Radin, E.L., 1985. Bone remodeling in response to in vivo fatigue microdamage. J. Biomech. 18, 189–200.
Burr, D.B., Forwood, M.R., Fyhrie, D.P., Martin, R.B., Schaffler, M.B., Turner, C.H., 1997. Bone microdamage and skeletal fragility in osteoporotic and stress fractures. J. Bone Miner. Res. 12, 6–15.
Cardoso, L., Herman, B.C., Verborgt, O., Laudier, D., Majeska, R.J., Schaffler, M.B., 2009. Osteocyte apoptosis controls activation of intracortical resorption in response to bone fatigue. J. Bone Miner. Res. 24, 597–605.
Cheung, W.Y., Liu, C., Tonelli-Zasarsky, R.M.L., Simmons, C.A., You, L., 2011. Osteocyte apoptosis is mechanically regulated and induces angiogenesis in vitro. J. Orthop. Res. 29, 523–530.
Cheung, W.-Y., Simmons, C.A., You, L., 2012. Osteocyte apoptosis regulates osteoclast precursor adhesion via osteocytic IL-6 secretion and endothelial ICAM-1 expression. Bone 50, 104–110.
Clarkin, C.E., Emery, R.J., Pitsillides, A.A., Wheeler-Jones, C.P., 2008. Evaluation of VEGF-mediated signaling in primary human cells reveals a paracrine action for VEGF in osteoblast-mediated crosstalk to endothelial cells. J. Cell. Physiol. 214, 537–544.
Dunstan, C.R., Somers, N.M., Evans, R.A., 1993. Osteocyte death and hip fracture. Calcif. Tissue Int. 53, S113–S117.
Ferrara, N., Gerber, H.-P., LeCouter, J., 2003. The biology of VEGF and its receptors. Nat. Med. 9, 669–676.
Frost, H.M., 1960. Presence of microscopic cracks in vivo in bone. Henry Ford Hosp. Med. Bull. 8, 25–35.
Goulet, G.C., Coombe, D., Martinuzzi, R.J., Zernicke, R.F., 2009. Poroelastic evaluation of fluid movement through the lacunocanalicular system. Ann. Biomed. Eng. 37, 1390–1402.
Harada, S., Nagy, J., Sullivan, K., Thomas, K., Endo, N., Rodan, G., Rodan, S., 1994. Induction of vascular endothelial growth factor expression by prostaglandin E2 and E1 in osteoblasts. J. Clin. Investig. 93, 2490.
Hazenberg, J.G., Freeley, M., Foran, E., Lee, T.C., Taylor, D., 2006. Microdamage: a cell transducing mechanism based on ruptured osteocyte processes. J. Biomech. 39, 2096–2103.
Henriksen, K., Neutzsky-Wulff, A.V., Bonewald, L.F., Karsdal, M.A., 2009. Local communication on and within bone controls bone remodeling. Bone 44, 1026–1033.
Herman, B.C., Cardoso, L., Majeska, R.J., Jepsen, K.J., Schaffler, M.B., 2010. Activation of bone remodeling after fatigue: differential response to linear microcracks and diffuse damage. Bone 47, 766–772.
Ito, H., Koefoed, M., Tiyapatanaputi, P., Gromov, K., Goater, J.J., Carmouche, J., Zhang, X., Rubery, P.T., Rabinowitz, J., Samulski, R.J., 2005. Remodeling of cortical bone allografts mediated by adherent rAAV-RANKL and VEGF gene therapy. Nat. Med. 11, 291–297.
Jacobs, C.R., Yellowley, C.E., Davis, B.R., Zhou, Z., Cimbala, J.M., Donahue, H.J., 1998. Differential effect of steady versus oscillating flow on bone cells. J. Biomech. 31, 969–976.
Kamel, M.A., Picconi, J.L., Lara-Castillo, N., Johnson, M.L., 2010. Activation of β-catenin signaling in MLO-Y4 osteocytic cells versus 2T3 osteoblastic cells by fluid flow shear stress and PGE_2: implications for the study of mechanosensation in bone. Bone 47, 872–881.
Keila, S., Kelner, A., Weinreb, M., 2001. Systemic prostaglandin E2 increases cancellous bone formation and mass in aging rats and stimulates their bone marrow osteogenic capacity in vivo and in vitro. J. Endocrinol. 168, 131–139.
Kennedy, O.D., Herman, B.C., Laudier, D.M., Majeska, R.J., Sun, H.B., Schaffler, M.B., 2012. Activation of resorption in fatigue-loaded bone involves both apoptosis and active pro-osteoclastogenic signaling by distinct osteocyte populations. Bone 50, 1115–1122.
Kidd, L.J., Stephens, A.S., Kuliwaba, J.S., Fazzalari, N.L., Wu, A.C.K., Forwood, M.R., 2010. Temporal pattern of gene expression and histology of stress fracture healing. Bone 46, 369–378.

Kitase, Y., Johnson, M.L., Bonewald, L.F., 2007. The protective effects of mechanical strain on osteocyte viability is mediated by the effects of prostaglandin on the cAMP/PKA and the beta-catenin pathways. J. Bone Miner. Res. 22, S178–S179.
Kurata, K., Heino, T.J., Higaki, H., Väänänen, H.K., 2006. Bone marrow cell differentiation induced by mechanically damaged osteocytes in 3D gel-embedded culture. J. Bone Miner. Res. 21, 616–625.
Liu, C., Zhao, Y., Cheung, W.Y., Gandhi, R., Wang, L., You, L., 2010. Effects of cyclic hydraulic pressure on osteocytes. Bone 46, 1449–1456.
Martin, R.B., 2003. Fatigue microdamage as an essential element of bone mechanics and biology. Calcif. Tissue Int. 73, 101–107.
Mori, S., Burr, D., 1993. Increased intracortical remodeling following fatigue damage. Bone 14, 103–109.
Mulcahy, L.E., Taylor, D., Lee, T.C., Duffy, G.P., 2011. RANKL and OPG activity is regulated by injury size in networks of osteocyte-like cells. Bone 48, 182–188.
Noble, B., Alini, M., Richards, R.G., 2003a. Bone microdamage and cell apoptosis. Eur. Cells Mater. 6, 46–55.
Noble, B.S., Peet, N., Stevens, H.Y., Brabbs, A., Mosley, J.R., Reilly, G.C., Reeve, J., Skerry, T.M., Lanyon, L.E., 2003b. Mechanical loading: biphasic osteocyte survival and targeting of osteoclasts for bone destruction in rat cortical bone. Am. J. Physiol. – Cell Physiol. 284, C934–C943.
O'Brien, F.J., Taylor, D., Dickson, G., Lee, T.C., 2000. Visualisation of three-dimensional microcracks in compact bone. J. Anat. 197, 413–420.
Parfitt, A., 1994. Osteonal and hemi-osteonal remodeling: the spatial and temporal framework for signal traffic in adult human bone. J. Cell. Biochem. 55, 273–286.
Phillips, J.A., Almeida, E.A.C., Hill, E.L., Aguirre, J.I., Rivera, M.F., Nachbandi, I., Wronski, T.J., van der Meulen, M.C.H., Globus, R.K., 2008. Role for β1 integrins in cortical osteocytes during acute musculoskeletal disuse. Matrix Biol. 27, 609–618.
Plotkin, L.I., Weinstein, R.S., Parfitt, A.M., Roberson, P.K., Manolagas, S.C., Bellido, T., 1999. Prevention of osteocyte and osteoblast apoptosis by bisphosphonates and calcitonin. J. Clin. Investig. 104, 1363–1374.
Ponik, S.M., Triplett, J.W., Pavalko, F.M., 2007. Osteoblasts and osteocytes respond differently to oscillatory and unidirectional fluid flow profiles. J. Cell. Biochem. 100, 794–807.
Raisz, L.G., Pilbeam, C.C., Fall, P.M., 1993. Prostaglandins: mechanisms of action and regulation of production in bone. Osteoporos. Int. 3, 136–140.
Reilly, G.C., 2000. Observations of microdamage around osteocyte lacunae in bone. J. Biomech. 33, 1131–1134.
Riddle, R.C., Donahue, H.J., 2009. From streaming potentials to shear stress: 25 years of bone cell mechanotransduction. J. Orthop. Res. 27, 143–149.
Robling, A.G., Bellido, T.M., Turner, C.H., 2006. Mechanical loading reduces osteocyte expression of sclerostin protein. J. Bone Miner. Res. 21, S72.
Schaffler, M., Choi, K., Milgrom, C., 1995. Aging and matrix microdamage accumulation in human compact bone. Bone 17, 521–525.
Schaffler, M., Pitchford, W., Choi, K., Riddle, J., 1994. Examination of compact bone microdamage using back-scattered electron microscopy. Bone 15, 483–488.
Shin, Y., Jeon, J.S., Han, S., Jung, G.-S., Shin, S., Lee, S.-H., Sudo, R., Kamm, R.D., Chung, S., 2011. In vitro 3D collective sprouting angiogenesis under orchestrated ANG-1 and VEGF gradients. Lab Chip 11, 2175–2181.
Silva, M.J., Uthgenannt, B.A., Rutlin, J.R., Wohl, G.R., Lewis, J.S., Welch, M.J., 2006. In vivo skeletal imaging of 18 F-fluoride with positron emission tomography reveals damage-and time-dependent responses to fatigue loading in the rat ulna. Bone 39, 229–236.
Smith, J.N., Calvi, L.M., 2013. Concise review: current concepts in bone marrow microenvironmental regulation of hematopoietic stem and progenitor cells. Stem Cells 31, 1044–1050.
Street, J., Lenehan, B., 2009. Vascular endothelial growth factor regulates osteoblast survival–evidence for an autocrine feedback mechanism. J. Orthop. Surg. Res. 4, 19.
Tan, S.D., de Vries, T.J., Kuijpers-Jagtman, A.M., Semeins, C.M., Everts, V., Klein-Nulend, J., 2007. Osteocytes subjected to fluid flow inhibit osteoclast formation and bone resorption. Bone 41, 745–751.
Tatsumi, S., Ishii, K., Amizuka, N., Li, M., Kobayashi, T., Kohno, K., Ito, M., Takeshita, S., Ikeda, K., 2007. Targeted ablation of osteocytes induces osteoporosis with defective mechanotransduction. Cell Metab. 5, 464–475.
Taylor, D., Clive Lee, T., 1998. Measuring the shape and size of microcracks in bone. J. Biomech. 31, 1177–1180.
Vashishth, D., Tanner, K., Bonfield, W., 2000a. Contribution, development and morphology of microcracking in cortical bone during crack propagation. J. Biomech. 33, 1169–1174.
Vashishth, D., Verborgt, O., Divine, G., Schaffler, M.B., Fyhrie, D.P., 2000b. Decline in osteocyte lacunar density in human cortical bone is associated with accumulation of microcracks with age. Bone 26, 375–380.
Verborgt, O., Gibson, G.J., Schaffler, M.B., 2000. Loss of osteocyte integrity in association with microdamage and bone remodeling after fatigue in vivo. J. Bone Miner. Res. 15, 60–67.
Waldorff, E.I., Christenson, K.B., Cooney, L.A., Goldstein, S.A., 2010. Microdamage repair and remodeling requires mechanical loading. J. Bone Miner. Res. 25, 734–745.
Xie, C., Ming, X., Wang, Q., Schwarz, E.M., Guldberg, R.E., O'Keefe, R.J., Zhang, X., 2008. COX-2 from the injury milieu is critical for the initiation of periosteal progenitor cell mediated bone healing. Bone 43, 1075–1083.
Yang, W.C., Harris, M.A., Heinrich, J.G., Guo, D.Y., Bonewald, L.F., Harris, S.E., 2009. Gene expression signatures of a fibroblastoid preosteoblast and cuboidal osteoblast cell model compared to the MLO-Y4 osteocyte cell model. Bone 44, 32–45.
You, L., Cowin, S.C., Schaffler, M.B., Weinbaum, S., 2001. A model for strain amplification in the actin cytoskeleton of osteocytes due to fluid drag on pericellular matrix. J. Biomech. 34, 1375–1386.
You, L., Temiyasathit, S., Lee, P., Kim, C.H., Tummala, P., Yao, W., Kingery, W., Malone, A.M., Kwon, R.Y., Jacobs, C.R., 2008. Osteocytes as mechanosensors in the inhibition of bone resorption due to mechanical loading. Bone 42, 172–179.